Environmental Chemistry

DOI: 10.1002/ange.200602453

Optical Sensors Based on Nanostructured Cage Materials for the Detection of Toxic Metal Ions**

Tatineni Balaji, Sherif A. El-Safty, Hideyuki Matsunaga, Takaaki Hanaoka, and Fujio Mizukami*

Chemical sensors are molecular receptors that transform their chemical information into analytically useful signals upon binding to specific guests. These sensors are attracting attention owing to their potential for easy detection and quantification of the pollutant species in many fields of application, such as waste management, environmental chemistry, clinical toxicology, and bioremediation of radionuclides.[1–6] Among these, the sensitive detection of heavy-metal ions, such as mercury and lead, is critical for monitoring the environment as they are highly toxic and common environmental pollutants. Although instrumental analyses such as atomic absorption or atomic emission spectroscopy are currently used in applications relevant to the detection of toxic metal ions, there is still a need to develop inexpensive and easy methods for the detection of these toxic ions. In view of these sophisticated experimental methods, emphasis is currently being placed on the development of sensor materials for the detection of toxic ions that offer high sensitivity,

[*] Dr. T. Balaji,[+] Dr. S. A. El-Safty,[+] Dr. H. Matsunaga, Dr. T. Hanaoka, Dr. F. Mizukami
National Institute of Advanced Industrial Science & Technology (AIST)
Research Center for Compact Chemical Process (CCP)
4-2-1, Nigatake, Miyagino-ku, Sendai 983-8551 (Japan)
Fax: (+81) 22-237-5226
E-mail: sherif.el-safty@aist.go.jp

[+] Both authors contributed equally to the practical work.

[**] We thank Dr. Y. Kiyozumi, Dr. T. Ikeda, and Dr. A. Kawai (CCP-AIST) for the measurements of Ar isotherms.

Supporting information for this article is available on the WWW under http://www.angewandte.org or from the author.

short response times, and selectivity.[7,8] Among all these sensor approaches, the optical sensors that allow on-site, real-time qualitative or semiquantitative detection without the use of any substantial or complicated spectroscopic instrumentation have received a great deal of attention as promising methods for the determination of pollutant species in environmental analysis.[9–11] However, most of the sensors developed so far were kinetically slow with a limited sensitivity for detection below the permissible level of toxic ions, indicating a lack of possibility to control the remote sensing of pollutant species.

With recent advances in mesostructured materials and nanotechnologies, new methods are emerging to design optical sensors and biosensors, and to develop highly sensitive solid-state sensors.[12–14] However, in recent years, large-scale nanostructured materials such as SBA-15 and MCM-41 have attracted significant interest for the development of optical chemical sensors.[15–19] Although these materials offer considerable advantages over other methods in the area of sensing technologies, there is still a growing demand to solve one of the major technological challenges in nano-optical sensors: the detection and determination of environmentally important toxic species at a low level of concentration with a rapid-assessment process. In this respect, we report herein the use of newly synthesized cubic *Fm3m* nanostructured cage-monolith-based optical sensors for highly sensitive and selective detection of Pb^{II}, Cd^{II}, Sb^{III}, and Hg^{II} toxic ions at subnanomolar concentrations in a few minutes. To the best of our knowledge, this is the first visual detection method to detect toxic ions at low-level concentrations based on the color change of the probe sensors (Scheme 1). Such cage monoliths with spherical nanosized cavities show evidence for a high adsorption capacity of probe molecules, efficient transport of toxic species through much more direct and easier diffusion to the network sites, and a high degree of detection functionality for these toxic ions without loss of cage character (i.e. uniformly shaped and sized cavity and entrance pores).

Instant direct-templating methods that apply a microemulsion system of F108 ($EO_{141}PO_{44}EO_{141}$) copolymer as a template were used to affect the rapid synthesis of highly ordered, and optically transparent cage silica monoliths (Scheme 1) with cubic *Fm3m* (HOM-C10) structures, as evidenced by X-ray diffraction (XRD) and N_2 isothermal profiles (see the Supporting Information).[20a,b] The potential use of these cage materials as colorimetric sensors **1**–**4** for the naked-eye detection of metal ions has generated considerable evidence for the accessibility and retainability of probe molecules in the three-dimensional cage cavity (Scheme 1). Several successful immobilization strategies that use direct and indirect postgrafting techniques of hydrophilic and hydrophobic chromophores into the cubic *Fm3m* cage monoliths were preformed to design sinklike sensors **1**–**4** (Scheme 2). However, the functionalized cage sensors were fabricated by following a direct immobilization for probe **1** and a two-step inclusion procedures for probes **2**–**4** through graft-controlled surface modification of the cage monoliths

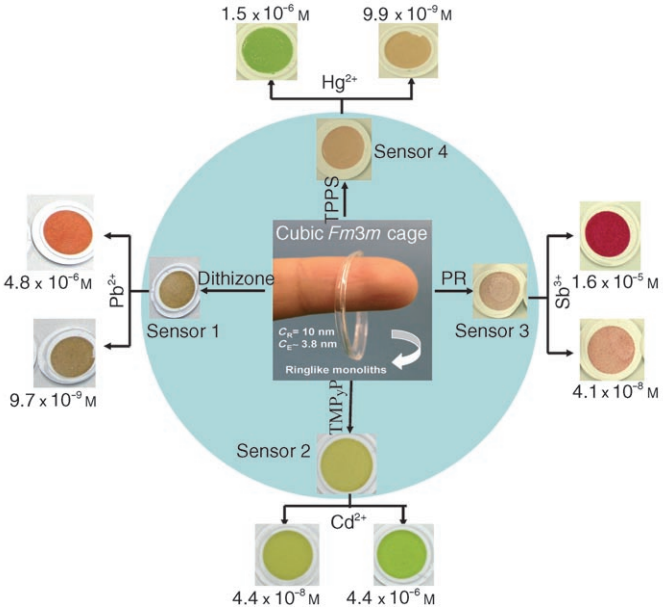

Scheme 1. A schematic representation of the colorimetric detection systems of optically monolithic cage sensors and the respective color changes over a tunable and wide detection range of the toxic analyte ions. C_R = pore cavity size, C_E = pore entrance size.

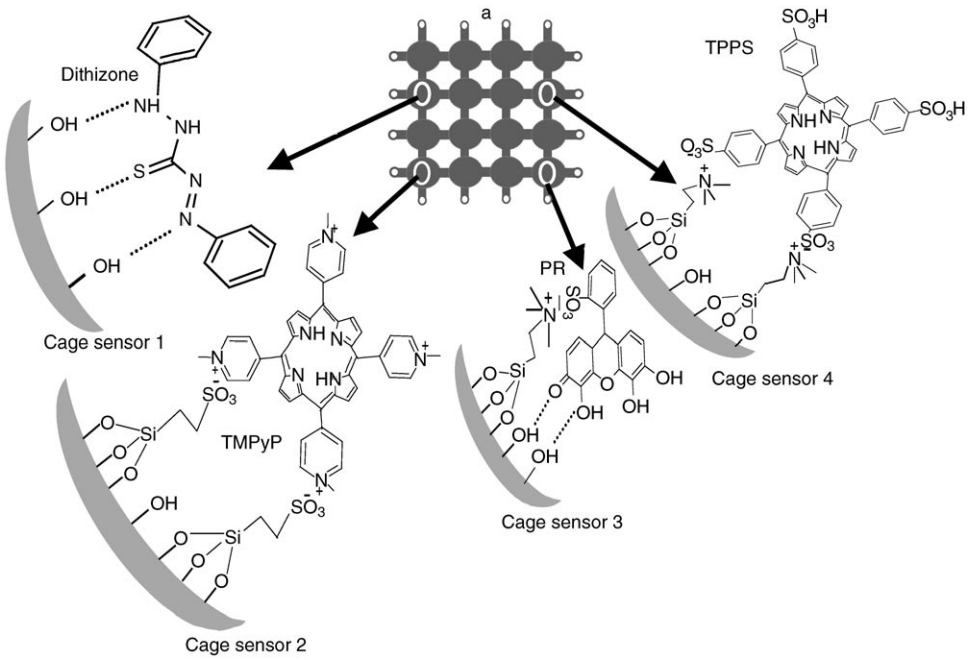

Scheme 2. Representative of the structures of the optical probe sinks **1**–**4** based on chromophore–cage cubic *Fm3m* nanostructures (a).

with amine- or thiol-coupling agents (see the Supporting Information). Our experimental results show that the coupling agents mercaptopropyl trimethoxysilane (MPTS) and *N*-trimethoxysilylpropyl-*N*,*N*,*N*-trimethylammonium chloride (TMAC) can be used to tune the polarity of the HOM surfaces on which the high accessibility of the α,β,γ,δ-tetrakis(1-methylpyridinium-4-yl)porphine *p*-toluenesulfonate (TMPyP), pyrogallol red (PR), and tetraphenylporphine tetrasulfonic acid (TPPS) moieties were observed (see Table 1 and the Supporting Information),[19,21,22] and therefore led to the generation of the long-term-stable sensors **2**, **3**, and **4** with a high selectivity for Cd^{II}, Sb^{III}, and Hg^{II} target ions, respectively, with sensitive detection and rapid-assessment analysis ($\leq$1 min).

In these sensing designs, despite the hydrophilic and hydrophobic character and grafting strategies of the immobilized probe moieties, the cage-monolithic materials exhibited higher adsorption integrity of the probes in terms of capacity and fast-loading kinetics than those of silica materials with amorphous or even-ordered structures (such as SBA-15).[20c] The excellent accessibility and functionality of the chromophore molecules into the 3D cubic *Fm*3*m* cage monoliths (see the Supporting Information) led to the creation of a new type of material for colorimetric detection, namely, optical probe sinks. This allowed for sensitivity over a wide and tunable detection range and simple detection by the naked eye without the use of high amounts of materials and annealing experiments (Scheme 1). To investigate the successful immobilizations of the probes without loss of the cage regularity and functionality, the optical probe sinks were characterized by a number of techniques such as ^{29}Si NMR spectroscopy, FTIR spectroscopy, thermogravimetric analysis (TG), and energy-dispersive X-ray (EDX) microanalysis (see the Supporting Information).[21,22] In general, our findings revealed that the chromophore moieties effectively bind to the HOM cage monoliths, as evidenced from the large adsorption value (Q) of the probe molecules (Table 1).

TEM images (Figure 1), in general, reveal well-organized mesopore arrays over a large area of the cubic *Fm*3*m* cage sensors, despite the harsh synthesis conditions required by batch contact–time experiments during the embedding/grafting techniques. Although the existence of undulating or curvelike channels was observed among the clear [110] and [111] incidences, which indicated the degree of distortion in the cage pores (Figure 1b), sufficiently large-scale ordered

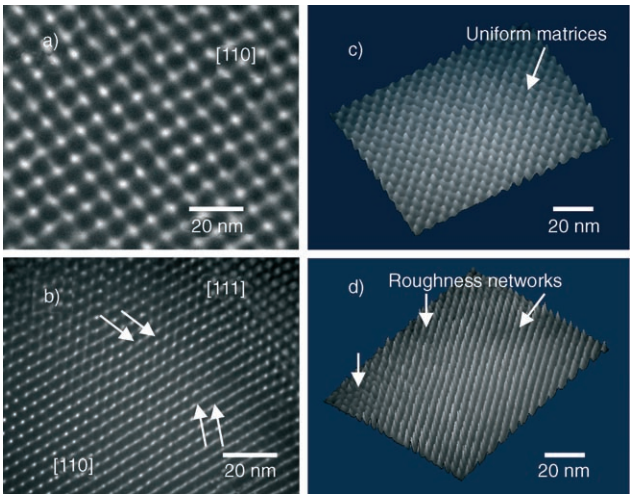

Figure 1. Representative TEM images of uniformly shaped cage mesochannels of the optical sensor **1** (a) and **2** (b) recorded along the [110] (a) and distorted [110]/[111] incidences (b). The 3D surfaces of these TEM micrographs (c and d) with a tilt of 45° revealed, in general, smooth and well-ordered network surfaces over wide-range domains. However, the TEM image (b) indicated that the grafting of the cage monoliths during the batch embedding experiments might induce the orientationally distorted portion, but this does not lead to significant collapse in the mesoscopic frameworks.

domains were retained for all cage-network surfaces. In addition, the regular and continuous extension in the network cage surfaces (Figure 1c,d) might permit the homogenous and fast diffusion of pollutant species into the sensing matrices.[23] AFM patterns (see the Supporting Information) clearly provide further evidence of topological defect-free surfaces associated with the organization of well-defined cagelike pores over large-scale regions. This indicates the retention of periodically ordered nanoscale cage structures with immobilization of the probe molecules (Scheme 2). Such retention led to a significant increase in the response time of the sensing systems ($\leq$1 min, Table 1), indicating the effectiveness of the 3D ordered pore surfaces of these optical probe sinks for facile transport of analyte ions during the detection process.

Figure 2 reveals that dominant face-centered cubic (fcc) *Fm*3*m* structures with a highly ordered structure and a large lattice constant in the range of 21–22 nm are characteristic of the sensors **1**–**4**. The well-resolved XRD patterns of sensor **1**–

Table 1: Structural parameters[a] of the optical-sensor-based cubic *Fm*3*m* cage monoliths, and characteristics of the sensing systems[b] during the colorimetric detection of toxic metal ions by using these cage probe sinks.

Optical sensors		a	C_R	S_{BET}	V_p	V_m	Q	$10^9\,D_L$	D_R	n	t [s]	pH range
Probe	Ions	[nm]	[nm]	[m^2g^{-1}]	[cm^3g^{-1}]	[cm^3g^{-1}]	[mmolg^{-1}]	[moldm^{-3}]	[moldm^{-3}]			
1	Pb^{2+}	22.0	14.9	702	1.05	0.1	0.012	2.38	9.7×10^{-9} to 4.8×10^{-6}	1:2	150	6–7.5
2	Cd^{2+}	21.2	14.3	500	0.90	0.05	0.0031	13.5	1.78×10^{-8} to 4.4×10^{-6}	1:1	40	7–10
3	Sb^{3+}	21.2	14.2	457	0.87	0.04	0.019	33.7	4.1×10^{-8} to 1.6×10^{-6}	1:1	60	2.7–3.6
4	Hg^{2+}	21.2	14.3	410	0.89	0.04	0.0054	6.34	9.9×10^{-9} to 1.5×10^{-6}	1:1	60	8–10

[a] Unit lattice constant ($a_{Fm3m}=d_{111}\sqrt{3}$), pore cavity sizes [$C_R=a\,(6/\vartheta\pi)^{1/3}(V_p\rho/1+V_p\rho+V_m\rho)^{1/3}$], where ϑ is the number of cavities in the unit cell; $\vartheta=4$ for cubic *Fm*3*m*, ρ is the density of the silica framework and equal to 2.2 gcm^{-3}, S_{BET} = specific surface area, and mesopore (V_p))/micropore (V_m) volumes. [b] Adsorption amount (Q) of the probe molecules at the saturation point within the cage structures, detection limit (D_L) and range (D_R), stoichiometry of the ion/chromophore complex formation (n), and kinetic responding times (t). S_{BET} = specific surface area.

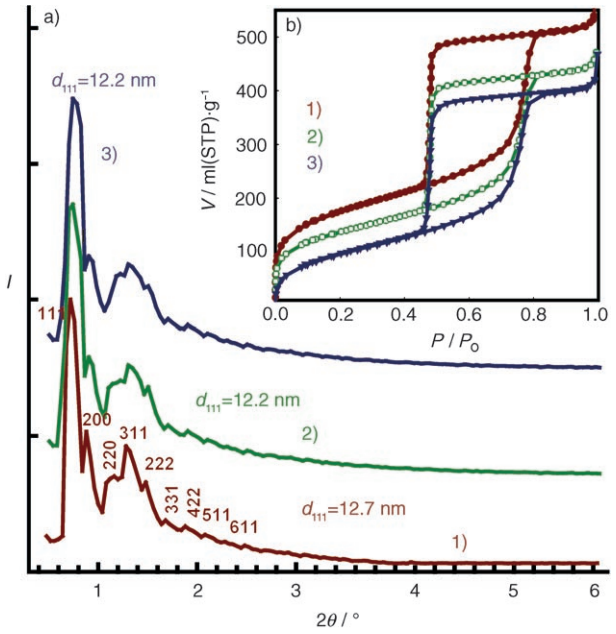

Figure 2. XRD patterns (a) and N_2 adsorption/desorption isotherms at 77 K (b) of cage sensors **1** (1), **2** (2), and **4** (3) before detection of Pb^{II}, Cd^{II}, and Hg^{II} analyte targets, respectively. STP = standard temperature and pressure.

4, which are similar to that of original cubic *Fm3m* cage monoliths HOM-C10 (see the Supporting Information),[20] provide strong evidence for a high degree of mesoscopically ordered sensors. The N_2 (Figure 2B and the Supporting Information) and Ar (see the Supporting Information) isothermal shapes indicated the stability of the cagelike pore domains with entrance sizes ≤ 5.0 nm (see reference [24] for extensive discussion). However, the decrease in the pore sizes of spherical cavities (Table 1) was observed by inclusion of the probe molecules and evidenced by the shift in the capillary condensation to a lower relative pressure P/P_o in both sets of N_2 and Ar isotherms (see the Supporting Information).[24] In addition, the decrease in the specific surface area and micropore/mesopore volumes (see Table 1) indicated that a large amount of the probes might be grafted into the large pore cavity; however, a significant amount might also anchor on the outer surfaces of the cage. It was evident that the cage character was maintained even after embedding of the sensing probe molecules, despite the extensive grafting process (Scheme 2). Such wide-range functionalities of the optical hybrid cage probes make these sensing systems technologically promising for colorimetric detection of toxic ions at a low concentration level, namely, subnanomolar (see Scheme 1).

The colorimetric detection of Pb^{II}, Cd^{II}, Sb^{III}, and Hg^{II} ions was revealed in the detection range of 9.9×10^{-9}–1.5×10^{-6} M by using the cage sensors **1**–**4**. The applicability of our sensing techniques, which are based on the design of 3D cage monoliths with the ability to act as an optical probe, was confirmed by the quantitative determination of these toxic metals (Scheme 1).[18,21] The color changes of the sensors **1**–**4**, induced by metal ions, can be easily visualized and quantified rapidly without any instrumentation, although UV/Vis spectroscopy was used for monitoring the changes in the absorption spectra that were observed when the metal ions complexed with the molecular probes (Figure 3). Although the cubic *Fm3m* cage structure had an influence on the color

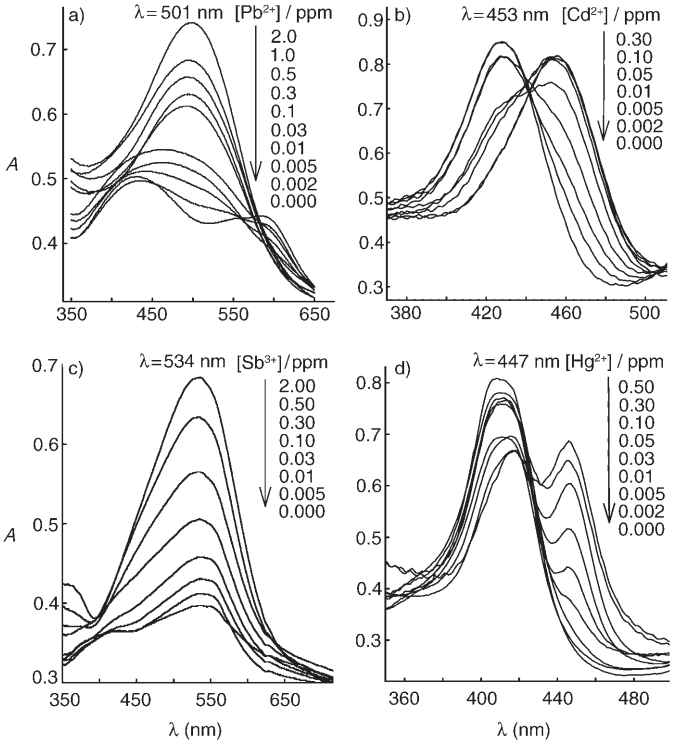

Figure 3. Concentration-dependent changes of UV/Vis absorption spectra of cage sensors **1** (a), **2** (b), **3** (c), and **4** (d) after detection of Pb^{II}, Cd^{II}, Sb^{III}, and Hg^{II} analyte targets, respectively.

changes of the sensors **1**–**4**,[18,21] these classes of cage sensing sinks offered several advantages in view of the long-term (several months) stability of the sensing probes[25] and the high adsorption capacity of the probes. This increases the utility of the probes as sensors in terms of sensitivity and fast kinetic detections.[6]

The ability to use naked-eye detection over the wide and tunable detection range of the analyte ions was clarified by UV/Vis spectroscopy (Figure 3). Our control experiments showed that sensitive colorimetric detection of metal ions required specific conditions, such as pH values and specific amounts of the cage sensor. The variation in these detection conditions was mainly dependent on the nature of the sensing system and the formation of the ion–chromophore complex (see Table 1). The calibration plots (see the Supporting Information) of these sensing systems show a liner correlation at low concentration ranges of analyte ions. However, in all detection designs, the liner correlation was varied depending upon the characteristics of the complex formation with the sensing systems. Furthermore, the stoichiometry of the metal–chromophore complexes can be derived from the deviation from linearity at the inflection point, as listed in Table 1.[18] From the calibration plot (see the Supporting Information),

the ion detection limit (D_L) of the cage sensors was estimated (Table 1).[18] In all sensing systems, the D_L values are the first evidence of a higher degree of sensitivity than ever previously reported for visual detection techniques.[8–18,21] This evidence confirms that the cage sensing monolithic designs can be used effectively to detect very low concentrations of toxic ions with very simple instrumentation or even the naked eye.

The key result in our study is that naked-eye detection was found to be possible for subnanomolar concentrations of metal ions (Scheme 1), although the interference of anionic and cationic species, namely, effective disturbance sensing, was influenced by the selectivity of the optical probe sinks.[21] The results herein show that the cage sensors **1**–**4** revealed highly selective sensing systems of Pb^{II}, Cd^{II}, Sb^{III}, and Hg^{II} target ions despite the presence of interference ions, such as cations, anions, or complexing agents, at concentrations up to 300 times that of analyte targets (for extensive studies, see the Supporting Information). In addition, no significant changes in the color developed maps of the chromophore–metal complexes were visually observed after the addition of effectively interfered ions, indicating that our sensing systems did not undergo integrated disturbance effects in their selective functions towards targets (see the Supporting Information).

The kinetic response was studied by continuously monitoring the colored complex spectra of cage sensors after the addition of analyte ions at varying times. Our results show that fast responding times t (where, $30\,s \le t \le 3$ min) were characteristic of the complexation reactions of the metal ions and chromophore probes in our sensing systems (Table 1). Spectrophotometric studies (data not shown) reveal that the optical density of the sensors reached the maximum plateau within a minute, indicating significant accessibility and diffusion of the analyte into the well-ordered probe sinks.[25,26] Despite the rapid response at high analyte concentrations in our sensing systems, the sensitive color detection, in particular at low analyte concentrations, was substantially influenced by the concentration of the chromophore (the amount of sensor used). Within these sensing systems, the amount of the sensors used ($\approx$2–5 mg) was optimized to find the ideal optical density and response time at low analyte concentrations.

Furthermore, the reusability and reproducibility of the cage sensors are of particular interest in developing recyclable hybrid optical sensors, highlighting their important characteristic features and desirability for industrial applications.[23] Both sets of parameters were extensively studied by repeated exquisite-detection regeneration cycles. In these treatment procedures, the use of specific concentrations of stripping agents, such as EDTA or Cl^-, SCN^-, and CN^- anions, made the removal of the metal ions (decomplexation) possible. For example, EDTA (0.1%) was an effective stripping agent for the removal of Pb^{II} from a complex with the dithizone probe (sensor **1**) without resulting in a reduced response. Our experiments show that more than four cycles of Pb^{2+} analyte removal resulted in a 90% reduction in the sensitive recognition (Figure 4). The decrease in the degree of sensitive recognition is due to the intensive effect of the stripping agents on the sensing functions during several cycles.[27]

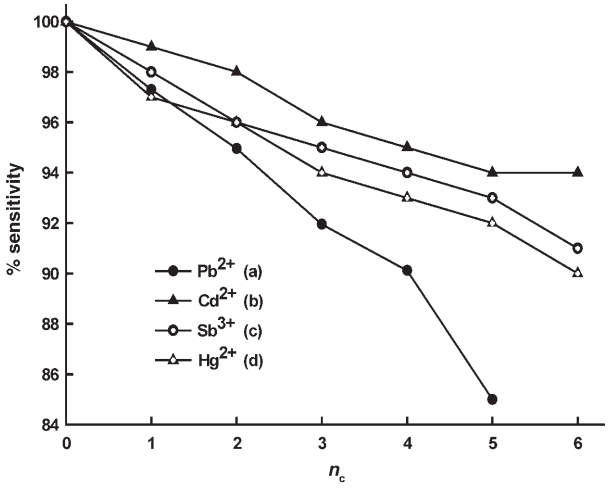

Figure 4. Reproducibility of the cage sensors **1** (a), **2** (b), **3** (c), and **4** (d) after complexation–regeneration cycles of analyte ions. Note the calculated percent variability with respect to the efficiency of the optical sensors after cycling of analyte ions (0.3 ppm). n_c = number of cycles.

In conclusion, cage monolithic silica materials with their uniformly nanosized cavities and entrances and highly ordered 3D cubic *Fm*3*m* structures show promise for the development of low-cost, rapid-response, and highly sensitive optical sensors. Our cage sensing systems exhibit exquisite sensitivity, long-term stability, and kinetically fast yet reliable detection of low concentrations (subnanomolar range) of several biologically toxic ions. These cage sensors could be used as optical sensing sinks that enable colorimetric detection (naked eye) with a high quantification limit. The effective use of these sensors as remote sensing operators on a real-time basis would significantly open up general and simple approachs for the identification of various biological and chemical toxic species without using sophisticated instruments.

Experimental Section

All materials were used without further purification. TMAC and MPTS were supplied from Gelest Co., Ltd. Japan. Diphenylthiocarbazone (dithizone), PR, TMPyP, and TPPS were obtained from Tokyo Kasei Kogyo Co., Ltd. Japan. Buffer solutions were prepared by mixing KCl/HCl (0.2 M) with CH_3COOH/CH_3COONa, 2-(cyclohexylamino)ethane sulfonic acid (CHES), 3-morpholinopropane sulfonic acid (MOPS), and *N*-cyclohexyl-3-aminopropane sulfonic acid (CAPS); a NaOH solution was employed to adjust the pH of the solutions (pH 6–10).

Fabrication of cubic *Fm*3*m* cage sensors: 1) Cage–dithizone sensor **1**: Dithizone was immobilized through direct dissolution and impregnation onto cubic *Fm*3*m* cage monoliths (HOM-C10) in ethanol. The stepwise impregnation was carried out under vacuum at 40 °C to reach probe saturation. The supported solid was washed with deionized water and dried at 80 °C.

2) Cage–TMPyP sensor **2:** The anchoring of MPTS onto the cage cavity was achieved by the addition of suspended MPTS to freshly prepared cubic *Fm*3*m* cage monoliths in refluxing toluene for 15 h.[28] The formation of cage-SO_3H monoliths was carried out by the addition of H_2O_2 (8%) solution to cage-SH materials at 50 °C with

continuous stirring for 15 h. The modified cage-SO_3H solid was filtered, washed with deionized water, and then dried at 60–70 °C for 5 h. The incorporation of the TMPyP chromophore was formed by addition of an aqueous solution of TMPyP (3.4×10^{-3} g L^{-1}) to 1 g of cage-SO_3H solid with continuous stirring for 3 h. The cage-TMPyP sensor **2** was collected by suction and washed with deionized water several times without resulting in elution of the TMPyP chromophore.

3) Cage–PR sensor **3:** The TMAC ligand was grafted into the cubic *Fm3m* cage cavity as previously described with the incorporation of MPTS. The immobilization of the PR chromophore onto cage-TMAC occurred under aqueous acidic conditions (pH ≈ 3) with continuous stirring for 2 h. The cage PR solid was collected and washed with acidified water to determine if there was any elution of the PR chromophore. The cage-PR sensor **3** was dried under vacuum at 65 °C for 5 h.

4) Cage–TPPS sensor **4**: The functionalized TPPS chromophore in cage-TMAC materials was preformed by addition of an aqueous solution of TPPS (2.8×10^{-6} g L^{-1}) to 1 g cage-TMAC solid under stirring for 4 h.[28] The cage-TPPS solid was collected and washed with deionized water several times and then dried in an oven at 65 °C for 5 h. Note that the adsorption capacity of the probe molecules at the saturation point (Table 1) was determined by monitoring the absorbance of the probe with the fabricated sensors.

Detection of metal ions by using cage sensors: Toxic metal ions, such as Pb^{II}, Cd^{II}, Sb^{III}, and Hg^{II}, were detected by using sensors **1**, **2**, **3**, **4** at various pH values (≈7, 9.5, 3, and 9) by using MOPS, CHES, HCl/KCl, and CAPS buffer solutions, respectively. pH Studies show that the color changes of the sensors were suitable at these specific pH values. All solid sensor monoliths were grinded into a fine powder, approximately 80–90 μm in size, before the detection of analyte ions was performed. The colorimetric detection was performed by mixing various concentrations of toxic ions to the solid sensors at a constant volume (20 cm^3) with shaking; after an interval of time (1–5 min) depending on the nature of the sensor systems, the solid sensors were collected by suction with cellulose acetate filter paper (25 mm; Sibata filter holder) or a 25-mm glass microfiber filter (lock-type syringe). The collected films were used for color assessment with the naked eye and for absorbance measurements with UV/Vis spectroscopy. The absorbance spectra of sensor **1** at 596 nm exhibited a blue shift to 501 nm through the addition of Pb^{II} ions. In sensing systems **2** and **4**, a bathchromic shift was revealed from 429 and 410 nm to 453 and 447 nm during the detection of Cd^{II} and Hg^{II} ions, respectively. However, absorbance spectra of sensor **3** showed a hyperchromic effect at 534 nm upon the addition of Sb^{III} ions. These results indicated the formation of charge-transfer complexes between the metal ions and the probes (Figure 4). The concentrations of toxic metal ions were calculated by comparing the color intensity of the target samples with that of the standard samples, which were prepared with known concentrations of ion solutions. Note that the elution of TPPS might be observed from the sensor **4** monoliths during the reaction with Hg^{II} ions, indicating the nature of the structural character of the TPPS chromophore on the formation of Hg^{II}/TPPS complex. To avoid this elution, the addition of TMAC solution (2 mL) to sensor **4** with stirring for 6 h was required.

Instrumentation: The metal ion concentration was determined with a Seiko SPS-1500 inductively coupled plasma atomic emission spectrometer (ICP-AES). The absorbance spectrum of the solid material was recorded by using a UV/Vis spectrometer (Shimadzu 3150, Japan). Small-angle powder XRD patterns were measured by using an MXP 18 diffractometer (Mac Science Co. Ltd.) with monochromated CuKα radiation. N_2 and Ar adsorption–desorption isotherms were measured by using a BELSORP36 analyzer (JP. BEL Co. Ltd) at 77 K. The surface area was measured by using the Brunauer–Emmett–Teller (BET) method, whereas the microporosity was assessed by using the α_s-plot method. The spherical cavity of the cage cubic *Fm3m* sensors was determined as previously reported.[24] Energy-dispersive X-ray microanalysis (DS-130S) was used to determine the elemental compositions. FTIR spectra were recorded with a Prestige-21 instrument (Shimadzu, Japan). TG analyses were conducted with Thermo Plus TG8120 (Rigaku, Japan). The AFM measurements were performed on a SPA300/SPI3700 (Seiko Instruments). TEM images were obtained by using a JEOL TEM (JEM-2000EXII) operating at 200 kV with a side-mounted CCD camera (Mega View III from Soft Imaging System Co.). ^{29}Si magic-angle spinning (MAS) NMR spectra were measured at room temperature on a Bruker AMX-500 spectrometer operatingat 125.78 MHz with a 90° pulse length of 4.7 μs. For all samples the repetition delay was 180 s with a rotor spinning at 4 kHz.

Received: June 19, 2006
Revised: August 9, 2006
Published online: October 9, 2006

Keywords: cage monoliths · colorimetry · environmental chemistry · sensors · toxic metal ions

[1] G. K. Walkup, B. Imperiali, *J. Am. Chem. Soc.* **1996**, *118*, 3053–3054.
[2] A. Miyawaki, J. Llopis, R. Helm, J. M. McCaffery, J. A. Adams, M. Ikura, R. Y. Tsien, *Nature* **1997**, *388*, 882–887.
[3] M. M. Henary, C. J. Fahrni, *J. Phys. Chem. A* **2002**, *106*, 5210–5220.
[4] J. Homola, S. S. Yee, G. Gauglitz, *Sens. Actuators B* **1999**, *54*, 3–15.
[5] F. Turner, *Science* **2000**, *290*, 1315–1317.
[6] P. Chen, C. He, *J. Am. Chem. Soc.* **2004**, *126*, 728–729.
[7] X. Wang, C. Drew, S. H. Lee, K. J. Senecal, J. Kumar, L. A. Samuelson, *Nano Lett.* **2002**, *2*(11), 1273–1275.
[8] R. Metivier, I. Leray, B. Valeur, *Chem. Eur. J.* **2004**, *10*, 4480–4490.
[9] E. Palomares, R. Vilar, J. R. Durrant, *Chem. Commun.* **2004**, 362–363.
[10] a) J. Liu, Y. Lu, *J. Am. Chem. Soc.* **2004**, *126*, 12298–12305; b) J. Liu, Y. Lu, *Anal. Chem.* **2004**, *76*, 1627–1632.
[11] J. M. Nam, C. S. Thaxton, C. A. Mirkin, *Science* **2003**, *301*, 1884–1886.
[12] E. Palomares, R. Vilar, A. Green, J. R. Durrant, *Adv. Funct. Mater.* **2004**, *14*, 111–114.
[13] J. Shi, Y. Zhu, X. Zhang, W. R. G. Baeyens, A. M. Garcia-Campana, *Trends Anal. Chem.* **2004**, *23*, 351–360.
[14] S. O. Obare, R. E. Hollowell, C. J. Murphy, *Langmuir* **2002**, *18*, 10407–10410.
[15] G. Wirnsberger, B. J. Scott, G. D. Stucky, *Chem. Commun.* **2001**, 119–120.
[16] L. Mercier, T. J. Pinnavaia, *Adv. Mater.* **1997**, *9*, 500.
[17] R. Metivier, I. Leray, B. Lebeau, B. Valeur, *J. Mater. Chem.* **2005**, *15*, 2965–2973.
[18] T. Balaji, M. Sasidharan, H. Matsunaga, *Anal. Bioanal. Chem.* **2006**, *384*, 488–494.
[19] a) A. B. Desacalzo, D. Jimenez, M. D. Marcos, R. M. Manez, J. Soto, J. El Haskouri, C. Guillem, D. Beltran. P. Amoros, M. V. Borrachero, *Adv. Mater.* **2002**, 14, 966; b) M. Boiocchi, M. Bonizzoni, L. Fabbrizzi, G. Piovani, A. Taglietti, *Angew. Chem.* **2004**, *116*, 3935–3940; *Angew. Chem. Int. Ed.* **2004**, *43*, 3847–3852; c) M. Comes, G. R. Lopez, M. D. Marcos, R. M. Manez, F. Sancenon, J. Soto, L. A. Villaescusa, P. Amoros, D. Beltran, *Angew. Chem.* **2005**, *117*, 2978–2982; *Angew. Chem. Int. Ed.* **2005**, *44*, 2918–2922.
[20] a) S. A. El-Safty, T. Hanaoka, F. Mizukami, *Chem. Mater.* **2005**, *17*, 3137–3145; b) S. A. El-Safty, T. Hanaoka, F. Mizukami, *J. Phys. Chem. B* **2005**, *109*, 9255–9264; c) D. Zhao, J. Feng, Q.

Huo, N. Melosh. G. H. Fredrickson, B. F. Chmelka, G. D. Stucky, *Science* **1998**, *279*, 548.
[21] C. W. Clavier, D. L. Rodman, J. F. Sinski, L. R. Allain, H.-J. Im, Y. Yang, J. C. Clark, Z-L. Xue, *J. Mater. Chem.* **2005**, *15*, 2356 – 2361.
[22] A. M. Liu, K. Hidajat, S. Kawi, D. Y. Zhao, *Chem. Commun.* **2000**, 1145 – 1146.
[23] a) J. Xiao, J. Wei, *Chem. Eng. Sci.* **1992**, *47*, 1123; b) L. Nicole, C. Boissiere, D. Grosso, P. Hesemann, J. Moreau, C. Sanchez, *Chem. Commun.* **2004**, 2312 – 2313.
[24] a) P. I. Ravikovitch, A. V. Neimark, *Langmuir* **2002**, *18*, 1550 – 1560; b) J. R. Matos, M. Kruk, L. P. Mercuri, M. Jaroniec, L. Zhao, T. Kamiyama, O. Terasaki, T. J. Pinnavaia, Y. Liu, *J. Am. Chem. Soc.* **2003**, *125*, 821 – 829; c) T. W. Kim, R. Ryoo, M. Kruk, K. P. Gierszal, M. Jaroniec, S. Kamiya, O. Terasaki, *J. Phys. Chem. B* **2004**, *108*, 11480 – 11489.
[25] M. Plaschke, R. Czolk, H. J. Ache, *Anal. Chim. Acta* **1995**, *304*, 107 – 113.
[26] L. Rodman, H. Pan, C. W. Clavier, X. Feng, Z.-L. Xue, *Anal. Chem.* **2005**, *77*, 3231 – 3237.
[27] A. Sayari, S. Hamoudi, Y. Yang, *Chem. Mater.* **2005**, *17*, 212 – 216.
[28] J. Evans, A. B. Zaki, M. Y. El-Sheikh, S. A. El-Safty, *J. Phys. Chem. B* **2000**, *104*, 10271 – 10282.

